

## NATURAL CONVECTIVE FLOWS: A COMPARISON WITH ELECTROVORTEX FLOWS

*J.L. Morón-Cruz, A. Beltrán\**

*Instituto de Investigaciones en Materiales, Unidad Morelia, Universidad Nacional Autónoma  
de México, 58190 Morelia, Mich. Mexico*

*\* e-Mail: albem@materiales.unam.mx*

This work studies the convection phenomenon of two different fluids confined in a cubic cavity with a side length of 50 mm. Experiments with water and GaInSn eutectic alloy are conducted by heating and cooling the bottom and top lids, respectively. Temperature differences of 2, 4, 6, and 8 K are imposed between both lids to study convective flows. Particle image velocimetry and ultrasonic Doppler velocimetry techniques are used to measure water flows, whereas for GaInSn only ultrasonic Doppler can be used. Additionally, a numerical study was conducted using the ANSYS Fluent software. Experiments and simulations predict time-dependent flow patterns for both fluids. Maximum velocity values for water and GaInSn are up to 6 and 12 mm/s, respectively. Values for GaInSn are in the same order of magnitude as those obtained for electrovortex flows in the same configuration.

### **Introduction.**

Thermal convection is a fundamental phenomenon in both natural and technological systems, playing a crucial role in stellar and solar convection [1], the Earth's geodynamo [2], and nuclear reactors [3]. Recently, understanding thermal convective flows has become particularly important in energy storage technologies like liquid metal batteries (LMB), which work with a stable density stratification of three conducting fluids, where flow dynamics influence heat and mass transfer [4, 5]. It is well known that the Prandtl number (Pr) governs the convective flow behavior. In particular, fluids like water (Pr = 7) exhibit well-defined boundary layers and oscillatory flow modes [6–8]. In contrast, low-Prandtl-number fluids (Pr  $\ll$  1), such as liquid metals, display rapid heat diffusion and distinct convective structures [9, 10]. For the LMB, cylindrical geometries have been extensively studied [11–13]. On the contrary, cubic configurations remain less explored despite their relevance to industrial prototypes [14]. This geometry introduces unique flow dynamics and is gaining attention due to its scalability.

Previous studies have debated the role of thermal convection in LMBs. Some studies suggest it has minimal influence [15, 16], whereas others argue that it significantly impacts transport phenomena [17–19]. In general, water is frequently used in convection experiments due to its transparency and well-characterized behavior. In studies related to electromagnetically driven flows, water-based electrolytes are sometimes employed as working fluids to simulate electrically conducting environments while maintaining optical accessibility [20, 21]. Despite their experimental advantages, significant differences in Prandtl number and thermal conductivity exist between water-based solutions and liquid metals, which must be considered when drawing direct comparisons.

The present paper studies, from an experimental and numerical point of view, convective flows of two fluids with contrasting Prandtl numbers: water (non-conducting) and GaInSn (electrically conducting). Using a cubic cavity setup, flow patterns are analysed with the Particle Image Velocimetry (PIV) and Ultrasonic Doppler Velocimetry (UDV) techniques. In addition to the experimental measurements and to fully understand the flow behavior, a three-dimensional numerical study was carried out. By directly com-

*Table 1.* Physical properties for the working fluids at  $T_\infty = 300$  K [22, 23].

Property	Deionized water	GaInSn
$\rho$ [kg/m <sup>3</sup> ]	997.1	6440
$\mu$ [mPa·s]	0.894	2.4
$\lambda$ [W/m K]	0.607	31
$C_p$ [J/kgK]	4181	370
$\beta$ [1/K]	$2.1 \times 10^{-6}$	$1.17 \times 10^{-4}$
$\sigma$ [S/cm]	$5.5 \times 10^{-10}$	$3.46 \times 10^4$
Pr	6.157	0.024

paring these fluid flows under identical conditions, this research is potentially relevant in LMB applications. Understanding the convective flow behavior in such systems is essential for improving heat and mass transfer efficiency, for reducing thermal stratification, and optimizing battery performance.

The paper is structured as follows: Section 1 describes the physical problem and experimental setup. Sections 2 and 3 outline the experimental and numerical methodologies, respectively. Section 4 presents and discusses the results; finally, Section 5 summarizes the conclusions and future research directions.

### 1. Physical problem.

The present study is conducted for two working fluids, distilled water and GaInSn, confined in a cubic cavity. It is made of acrylic with a side length  $L$  of 50 mm. Two similar copper plates are used as bottom and top lids. Two Peltier cells, in contact with the outermost external surface of the plates, are connected to an electronic control system. With a Python code, it is possible to keep the plates at a constant temperature.

Physical properties for both fluids are shown in Table 1.

Across the copper plates, a constant temperature is set by applying a hot temperature  $T_H$  at the bottom and a cold one  $T_C$  at the top, thus having a temperature difference  $\Delta T$  in the fluid. Four different values are explored,  $\Delta T = 2, 4, 6,$  and  $8$  K.

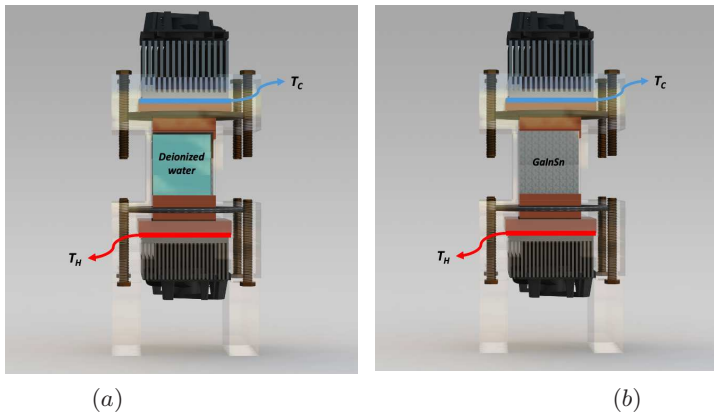


*Fig. 1.* Sketch of the experimental setup, not drawn to scale. Frontal view of the vessel. The cubic cavity is filled with (a) deionized water and (b) GaInSn. Both are subject to an axial temperature difference.

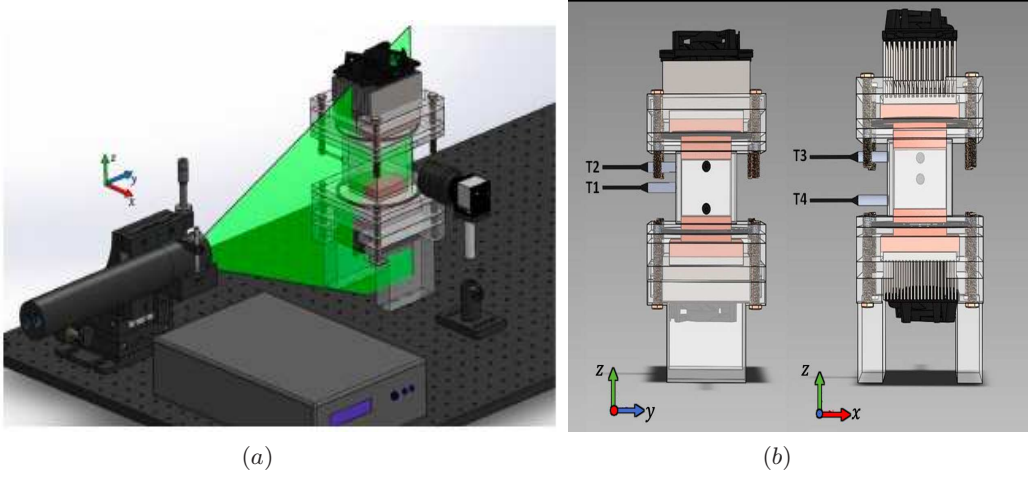


Fig. 2. CAD models for experimental measurements: (a) PIV setup for water, (b) UDV setup for GaInSn.

## 2. Experimental methodology.

In this study, Particle Image Velocimetry (PIV) and Ultrasonic Doppler Velocimetry (UDV) are used to measure convective flows. Due to water transparency, only PIV is employed, whereas UDV is used for both water and the opaque GaInSn alloy. The origin of the coordinates is located at the center of the bottom cap. The  $z$ -coordinate represents the vertical direction aligned with gravity;  $x$ - and  $y$ -axes lie in the horizontal plane, with the  $x$ -axis along the front-back direction and the  $y$ -axis along the left-right direction. The velocity components in the  $x$ ,  $y$ , and  $z$  directions are  $u$ ,  $v$ , and  $w$ , respectively.

For water, the fluid motion is analyzed in a plane illuminated by a 532 nm laser (Z-laser Z40M18BF), emitting a continuous 40 mJ sheet with a thickness of  $7 \times 10^{-4}$  m. This measurement plane is oriented in the  $(y, z)$  plane and positioned at the cavity's center at  $x=0$ , as shown in Fig. 2a. Polyamide tracer particles with a  $50 \mu\text{m}$  diameter and density of  $1120 \text{ kg/m}^3$  are used to track the fluid motion. A CCD camera (Imaging Source DMK 23U618) captures the trajectory at 30 fps over a 6-minute duration. The camera is positioned 0.15 m from the measurement plane and records images at  $640 \times 480$  pixels resolution. Post-processing uses the software Dantec Dynamic Studio 5.1 with interrogation areas of  $32 \times 32$  pixels and 50% overlap. Velocity vectors are obtained via cross-correlation of consecutive image pairs and further refined through standard validation, filtering and smoothing techniques [20], [21].

Due to the opacity of GaInSn, velocity measurements rely solely on Ultrasonic Doppler Velocimetry (UDV) using a Signal-Processing DOP 4000 system with 8 MHz probes (TR0805SS). Measurements are made at four transducer locations, as illustrated in Fig. 2b. The T1 measures the  $v$ -component at the midpoint of the vessel's width; T2 is positioned 12 mm below the top lid, measuring  $v$  near a vertical wall; T3 is placed 12 mm from the sidewall, measuring the  $u$ -component near the front face; and T4 is located 12 mm above the bottom lid, also measuring the  $u$ -component parallel to T3.

The T2, T3, and T4 provide insight into the flow behavior near the vertical boundaries, where convection is expected to be strongest. The T1 captures the velocity component in the middle of the cavity, offering information on bulk flow dynamics.

### 3. Numerical methodology.

In addition, for a better understanding of the flow behavior, a three-dimensional numerical study was carried out in the ANSYS Fluent v19.2 software. To simulate the problem under study, the fluids are considered Newtonian and incompressible. Mass, momentum, and energy conservation equations are solved. Time-dependent laminar simulations were performed. The SIMPLEC algorithm was used for pressure-velocity coupling. The meshing strategy, boundary conditions, and solver settings are described in the following.

The inner volume of the cavity is extracted from the CAD design. It represents the fluid-filled region, where the flow and transport equations are solved. In addition to the internal volume, solid volumes representing the vertical copper plates were also considered.

A computational mesh with 575588 elements was constructed using the SalomeMeca software, see Fig. 3. This mesh is called a fine mesh, and it considers both the solid and the fluid domains.

To simulate the experimental conditions, the no-slip condition for the velocity was applied at all solid surfaces. At the outermost external faces of the upper and bottom copper plates, a Dirichlet condition was fixed with  $T = T_C$  and  $T_H$ , respectively. The side walls of the internal volume were considered adiabatic.

### 4. Results and discussion.

To explore the dynamics of the flows in detail, a frequency analysis was conducted using the enhanced temporal resolution of UDV technique. Specifically, experimental and numerical velocity values were extracted at a fixed position ( $x = 0$ ,  $y = 15$  mm, and  $z = 24$  mm), corresponding to the T4 probe. Notably, the acquired signals exhibited oscillatory values, reflecting the inherent fluctuations of the flows during the measurements (see Fig. 4).

For each flow configuration, a Fast Fourier Transform (FFT) analysis was applied to determine the characteristic frequency ( $f$ ) and its corresponding period. This characteristic frequency was identified by locating the dominant peak in the power spectral density of the velocity signals. A comparison between experimental and numerical results (not shown) reports a slight variation of 5 to 10%, confirming the reliability of the numerical simulations.

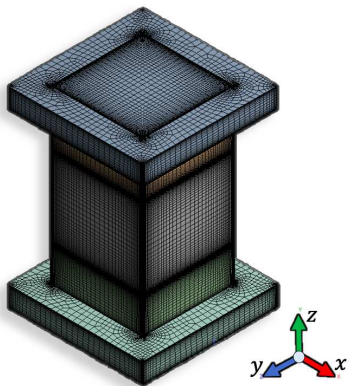


*Fig. 3.* Isometric view of the computational mesh for both liquid and solid domains.

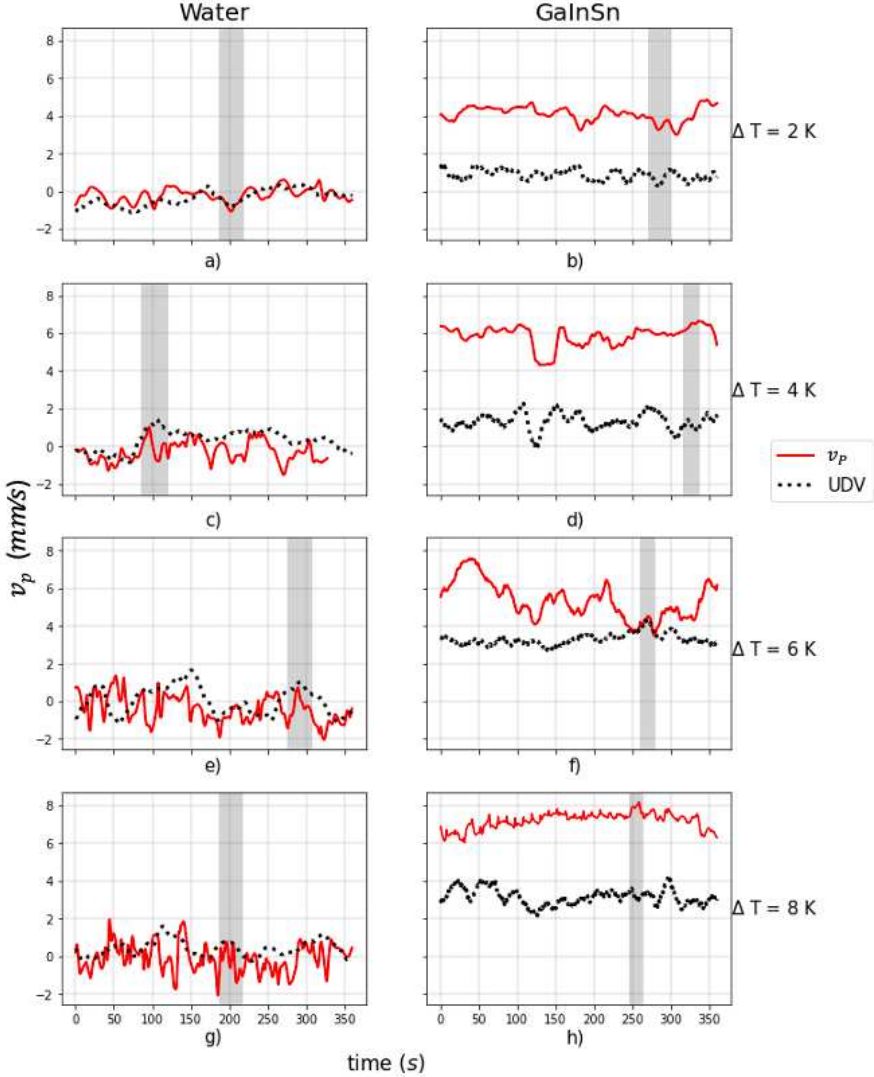


Fig. 4. The  $v$ -component of the velocity at  $y = 15 \times 10^{-3}$ ,  $z = 24 \times 10^{-3}$ , and  $x = 0$  m ( $v_p$ ) vs. time. The shaded area corresponds to the characteristic period, where the velocity fields and profiles are averaged.

Using the characteristic period as a reference, a time interval was carefully selected to maximize the alignment between the numerical and experimental velocity signals. With the characteristic frequency  $f$  and the maximum velocity  $U_m$ , the Strouhal number was calculated as follows:

$$St = \frac{fL}{U_m}. \quad (1)$$

where  $L$  is the characteristic length of the cavity. This approach allows a dimensionless comparison of the oscillatory behavior as a function of the Rayleigh number.

As seen in Fig. 5, a similar behavior for both fluids is observed. For water,  $St$  falls

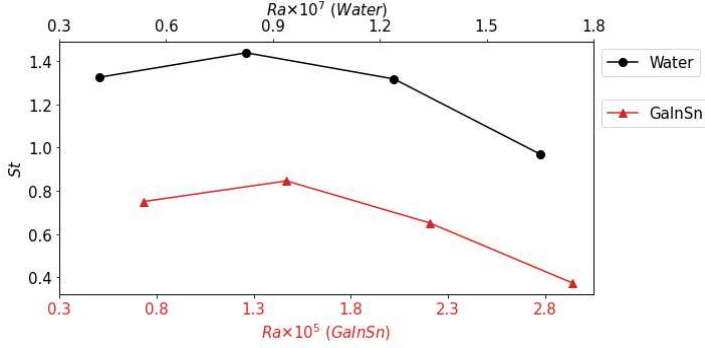


Fig. 5. Strouhal number vs. Rayleigh number for: (a) water, (b) GaInSn.

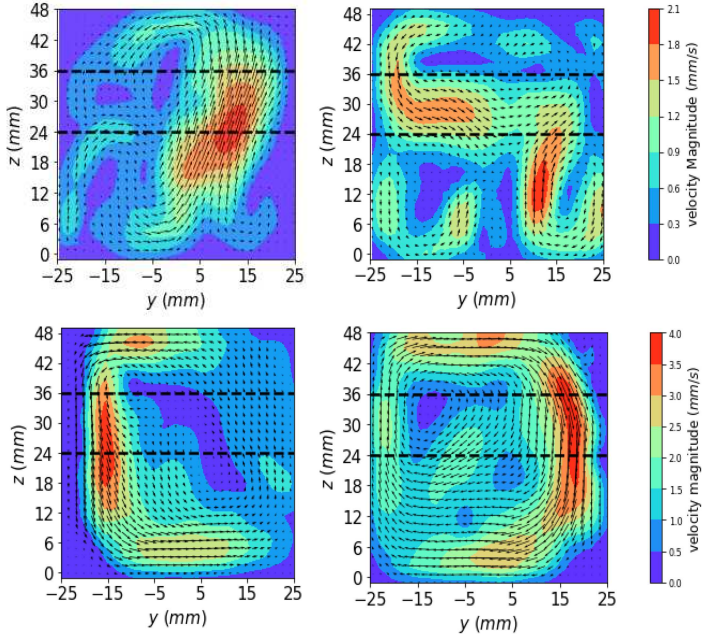


Fig. 6. Experimental results for the average velocity fields and velocity magnitude contours obtained from PIV for  $Ra$  numbers: (a)  $4.125 \times 10^6$ , (b)  $8.251 \times 10^6$ , (c)  $1.237 \times 10^7$ , and (d)  $1.650 \times 10^7$ . The black lines represent the transducer levels for UDV.

within the range of  $0.8 < St < 1.3$ , which represents a transition of the flow domain initially by local acceleration and subsequently by convective acceleration. Whereas, for GaInSn, a full convective acceleration domain is shown.

4.1. Water flows. Fig. 6 shows a comprehensive portrayal of the flow behavior under varying temperature differences for water. Both experimental and numerical data are presented in terms of the Rayleigh number defined by

$$Ra = \frac{g \beta (T_H - T_C) L^3}{\nu \alpha},$$

where  $g$  is the acceleration due to gravity,  $\beta$  is the thermal expansion coefficient,  $\nu$  is the kinematic viscosity, and  $\alpha$  is the thermal diffusivity.

For temperature differences of  $\Delta T = 2$  and  $4$  K, the velocity fields exhibit recircula-

tion zones within the  $(y, z)$ -plane. The central region emerges as a zone of heightened velocity magnitudes, with values soaring up to 2.1 mm/s. As we delve further into the spectrum of temperature differences, namely,  $\Delta T = 6$  and 8 K, an alternate phenomenon comes to the fore. Here, a recirculating flow pattern dominates, spanning the entire  $(y, z)$ -plane. The recirculation near the walls should be pointed out that is coupled with its central counterpart and reaches up to 4 mm/s.

To provide a rigorous quantitative assessment of the influence of temperature differences on flow patterns and to facilitate an insightful comparison between our measurement techniques, velocity profiles were extracted from the aforementioned average fields.

In general, Fig. 7 shows a good comparison between PIV and UDV techniques. Notably, within the context of the T1 probe, a remarkable agreement in orders of magnitude is evident. An asymmetric shape along the  $z$ -velocity axis suggests upward and/or downward flows along the walls adjacent to the cavity.

For T2, the profiles observed harmonize seamlessly with our earlier predictions. In

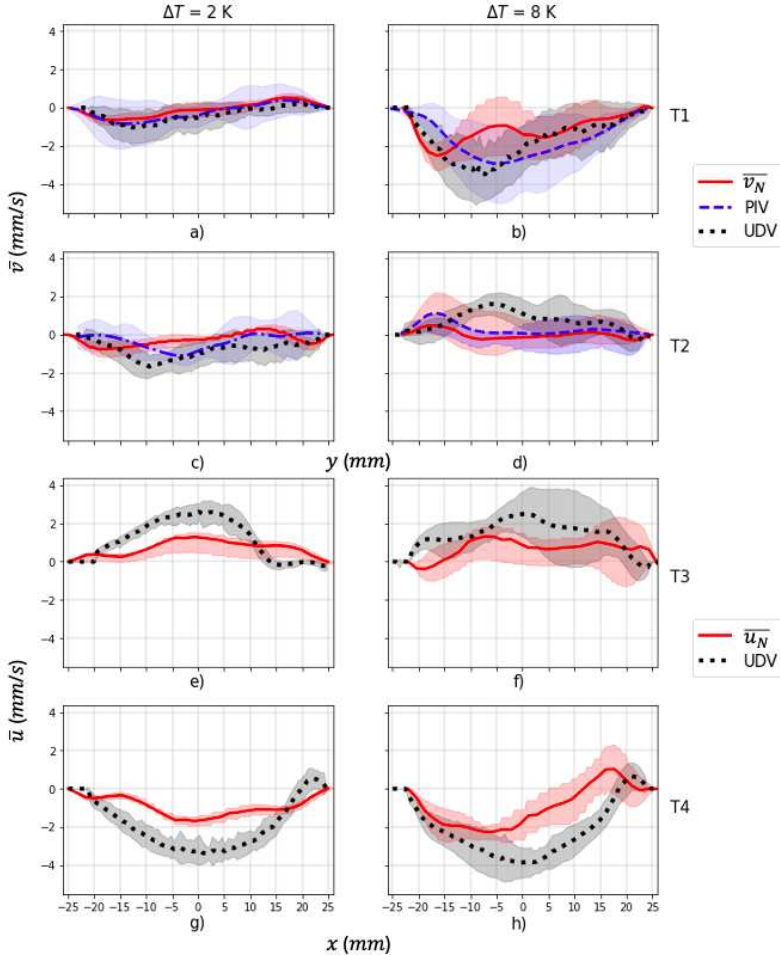
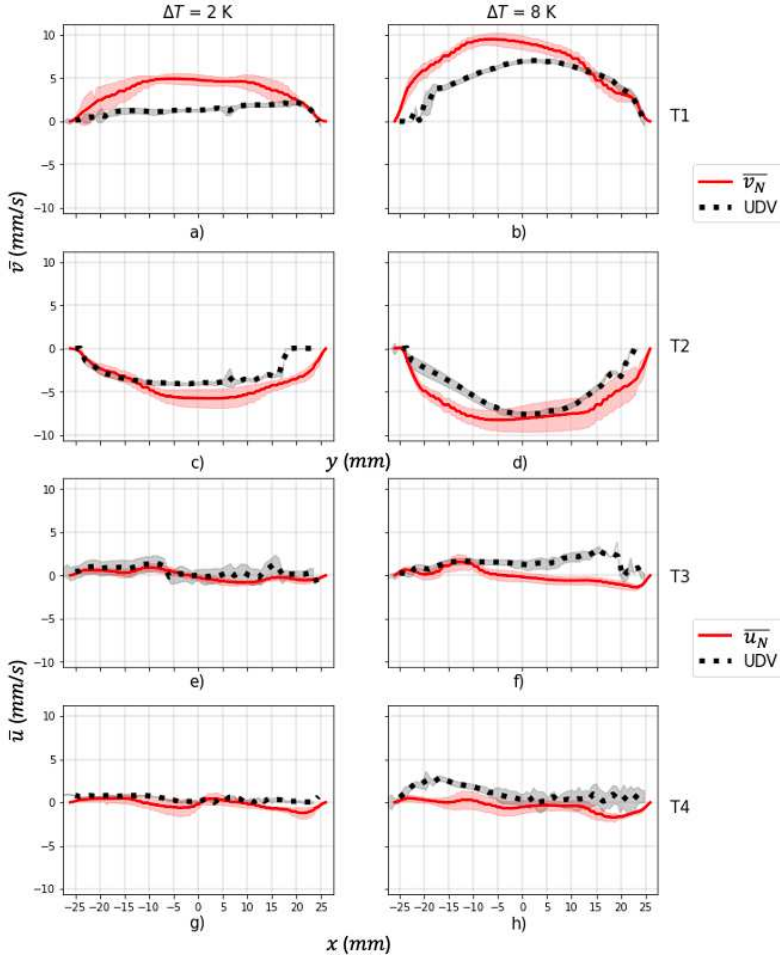


Fig. 7. For water, a comparison between the experimental velocity profiles extracted from PIV with those measured with UDV and the ones obtained from simulations ( $u_N$  and  $v_N$ ).

particular, for  $\Delta T$  values of 2 and 4 K, the profiles distinctly show lower velocities, consistent with expectations. Strikingly, as the temperature difference increases to  $\Delta T = 6$  and 8 K, the velocity reaches up to 5 mm/s.

For the average profiles from T3 and T4, only UDV and numerical results are showcased. Remarkably, the velocity magnitudes are depicted only in one direction for the numerical and experimental solutions, although disparities in magnitude are evident. Specifically, the experimental solution showcases elevated magnitudes in the central region of the cavity, featuring maximum velocities spanning a range of 2 to 5 mm/s. With the T3 and T4 probes situated near the vertical walls, the flow's distinctive recirculating flow behavior is inferred, marked by a sizable cell concentrated along the cavity walls. However, given the absence of measurements within the central zone, a definitive conclusion regarding this behavior remains elusive.

**4.2. GaInSn flows.** Average velocity profiles were calculated from probes T1, T2, T3, and T4. They were compared with those obtained from the simulations. A remarkable consistency emerges, starting with the T4 probe. The average profiles for T4



*Fig. 8.* For GaInSn, a comparison between the experimental velocity profiles extracted from PIV with those measured with UDV and the ones obtained from simulations ( $u_N$  and  $v_N$ ).

exhibit a unidirectional flow pattern, with entirely positive velocities diminishing near the cavity walls. This distinctive behavior yields velocities ranging from 2 to 7 mm/s in the experimental domain, aligning commendably with the numerical solution. For the T3 probe, a good comparison between simulations and measurements becomes more evident. Similar to T4, an increase in velocity magnitudes correlates with the escalating temperature differences.

T3 profiles reveal velocities ranging from  $-4$  to  $-10$  mm/s, underscoring the influence of temperature gradients. An analysis of both T3 and T4 profiles reveals a flow recirculation in the  $(y, z)$ -plane, the velocity fields from the simulations confirm this behavior. It is noteworthy that there is a clear increase in velocity magnitude with Ra. The no-slip condition at the walls causes flow patterns to reach high velocities in the bulk, with stronger flows leading to increased velocities near the walls, consistent with the expected motion. For T1 and T2, a distinct divergence in velocity values compared to the  $(y, z)$ -plane is observed. The velocity profiles exhibit an asymmetrical disposition, with subdued velocities within the cavity's central region ranging between  $-1.5$  and  $1.5$  mm/s. This behavior partially aligns with the simulation outcomes, showcasing the robustness of our analysis across different measurement scenarios. Significantly, our findings are in agreement with the study conducted by Cheng *et al.* [12], where recirculation reaches velocities of 12 mm/s.

**4.3. Nusselt number.** For a comprehensive evaluation of heat transfer dynamics, the Nusselt number Nu was numerically evaluated. The calculation procedure was as follows: for each instant of time, the average total heat flux at the bottom interface and the average temperature difference between the bottom and the top interfaces were directly obtained from the software. With these two parameters, the convective heat transfer coefficient  $h$  was obtained. The Nu was calculated as  $Nu = hL/\lambda$ . For water and GaInSn, the results are shown in Figs. 10a,b, respectively. These plots show Nu values

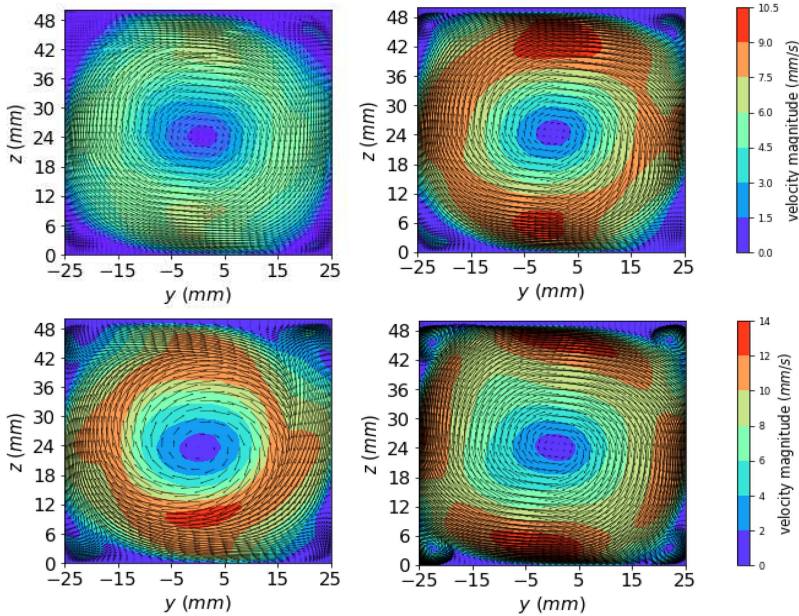


Fig. 9. Numerical average velocity fields and velocity magnitude isocontours for different Ra numbers: (a)  $7.345 \times 10^4$ , (b)  $1.469 \times 10^5$ , (c)  $2.203 \times 10^5$ , and (d)  $2.938 \times 10^5$ .

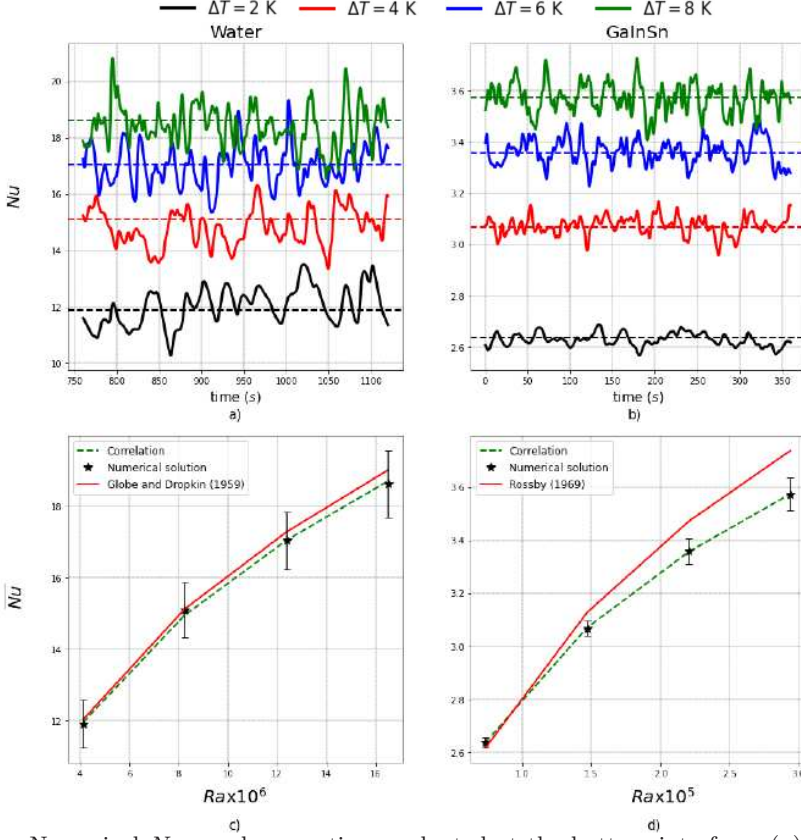


Fig. 10. Numerical  $Nu$  number vs. time evaluated at the bottom interface: (a) water and (b) GaInSn. Time-averaged  $Nu$  number vs. Rayleigh number and its comparison with reported correlations: (c) water and (d) GaInSn.

as a function of time for different temperature difference values.

To compare with reported correlations, the time-averaged  $Nu$  number  $\overline{Nu}$  was calculated from the signals reported in Figs. 10a,b. For GaInSn, the results were compared with a correlation reported by Rossby [24]:

$$Nu = 0.147Ra^{0.257}$$

(valid in the range of  $10^3 < Ra < 5 \times 10^5$  for mercury).

For water, the results were compared with the correlation given by Globe and Dropkin [25]:

$$Nu = 0.069Ra^{0.33} Pr^{0.074}$$

(valid in the range of  $1.5 \times 10^5 < Ra < 4 \times 10^7$  for any fluid).

Notably, both equations agree well with the numerical results, as shown in Fig. 10.

Based on the numerical results, the following  $\overline{Nu}(Ra)$  correlations for water and GaInSn are reported:

$$\begin{aligned} \overline{Nu} &= 0.087Ra^{0.323}, \\ \overline{Nu} &= 0.226Ra^{0.219}. \end{aligned}$$

For water,  $\overline{\text{Nu}}$  spans a range from 10.9 to 18.6, whereas for GaInSn, it reaches a modest increment, ranging from 2.4 to 3.2.

*4.4. Convective and electrovortex flows.* There is disparity of opinions regarding the importance of thermal convection in the operation of these batteries. Shen and Zikanov [15], for instance, argue that “the risk of interface rupture in an LMB due to convection flow should be considered irrelevant”, a claim supported by Keogh [16]. Conversely, Personnetaz *et al.* [17] highlight that in realistic LMBs with thin electrolyte layers (5 mm), thermal convection will prevail in the negative electrode. Kelley and Sadoway [18] suggest that heating at the base could lead to millimeter-scale velocities in the electrode, consistent with previous findings by the research group [19]. This study reports velocity magnitudes on the millimeter scale, comparable to previous studies on electrovortex flow conducted by the research group in a similar configuration [26]. It is suggested that convection may be equally relevant as electrovortex flow in LMBs. However, a more precise study addressing both flows simultaneously is necessary since it has been reported that, with sufficiently high currents, electrovortex flow dampens thermal convection flow. Confirming these observations is expected in future studies.

## 5. Concluding remarks.

In summary, the experimental investigation conducted in this study shed light on the dynamics of natural convection in both electrically conducting (GaInSn) and non-conducting (water) fluids confined within a cubic cavity subjected to varying temperature differences.

The obtained results revealed intriguing relationships between temperature differentials and characteristic flow periods, highlighting the intricate interplay between thermal conditions and flow behavior. For water, localized recirculations were observed in the cavity’s central zone at lower temperature differences, while higher differences resulted in increased flow velocities near the walls, forming larger cells with smaller recirculations confined to the corners. Both experimental and numerical results exhibited a qualitative agreement, with velocity profiles indicating a direct correlation between the temperature difference and the velocity magnitude, reaching up to  $6 \times 10^{-3}$  m/s.

For GaInSn, the velocity profiles indicated a predominantly uniform flow along the  $z$ -direction, albeit with indications of recirculation in the  $(y, z)$ -plane, particularly near the cold wall. Numerical simulations also supported experimental observations, suggesting more complex flow patterns. Velocity magnitudes reached up to  $12 \times 10^{-3}$  m/s, twice those reported for water.

Furthermore, a heat transfer study yielded Nusselt number correlations for both fluids, exhibiting behaviors consistent with the literature.

This study supports recent claims indicating that convection may be equally relevant as electrovortex flows in LMBs emphasizing the need for further investigation to understand the simultaneous effects of both flows.

**Acknowledgments.** Financial support from the CONAHCyT CF-2023-I-1373 and UNAM-DGAPA-PAPIIT IN107722 projects is gratefully acknowledged. J.L. Morón-Cruz thanks a grant from CONAHCYT. Experimental characterization was performed at the Magnetohydrodynamic Laboratory, whereas the computations were performed at the Laboratory for Design, Modeling, and Simulations (LDMS), both at the Morelia Unit of the IIM-UNAM. The authors thank Alejandro Pompa for the HPC support as well as Dr. Guillermo Ramírez-Zúñiga and Dr. Salvador Escobar from UTEZ and ICF-UNAM, respectively, for their help with experimental instrumentation.

## References

- [1] E.A. SPIEGEL. Thermal turbulence at very small prandtl number. *Journal of Geophysical Research (1896-1977)*, vol. 67 (1962),no. 8, pp. 3063–3070.
- [2] U. CHRISTENSEN AND J. AUBERT. Scaling properties of convection-driven dynamos in rotating spherical shells and application to planetary magnetic fields. *Geophys. J. Int.*, vol. 166 (2006), pp. 97–114.
- [3] D. SIKORSKA, *et al.* Convective heat transfer in pwr, bwr, candu, smr, and msr nuclear reactors-a review. *Energies*, vol. 17 (2024).
- [4] D. KELLEY AND T. WEIER. Fluid Mechanics of Liquid Metal Batteries. *Applied Mechanics Reviews*, vol. 70 (2018), no. 2, p. 020801.
- [5] T. WEIER. *Liquid metal batteries*,(2021).
- [6] D. FUNFSCHILLING AND G. AHLERS. Plume motion and large-scale circulation in a cylindrical Rayleigh-Bénard cell. *Phys. Rev. Lett.*, vol. 92 (2004), p. 194502.
- [7] Q. ZHOU, *et al.* Oscillations of the large-scale circulation in turbulent Rayleigh-Bénard convection: the sloshing mode and its relationship with the torsional mode. *Journal of Fluid Mechanics*, vol. 630 (2009), p. 367–390.
- [8] J. NÚÑEZ, A. BELTRÁN, AND M. RIVERO. Natural convection in a partially heated cylinder: A numerical study. *Journal of Theoretical and Applied Mechanics*, vol. 59 (2021), no. 4, pp. 623–636.
- [9] J. SCHUMACHER, P. G OTZFRIED, AND J. SCHEEL. Enhanced enstrophy generation for turbulent convection in low-prandtl-number fluids. *Proceedings of the National Academy of Sciences of the United States of America*, vol. 112 (2015).
- [10] J. AURNOU, *et al.* Rotating convective turbulence in earth and planetary cores. *Physics of the Earth and Planetary Interiors*, vol. 246 (2015), pp. 52–71.
- [11] J. CHENG, *et al.* Laboratory model of electrovortex flow with thermal gradients for liquid metal batteries. *Experiments in Fluids*, vol. 63 (2022), no. 11.
- [12] J. CHENG, *et al.* Oscillations of the large-scale circulation in experimental liquid metal convection at aspect ratios 1.4-3. *Journal of Fluid Mechanics*, vol. 949 (2022), p. A42.
- [13] P. PERSONNETTAZ, T.S. KLOPPER, N. WEBER, AND T. WEIER. Layer coupling between solutal and thermal convection in liquid metal batteries. *International Journal of Heat and Mass Transfer*, vol. 188 (2022), p. 122555.
- [14] D.J. BRADWELL, G. CEDER, L. ORTIZ, AND D.R. SADOWAY. *Liquid metal alloy energy storage device* (US Patent 9,076,996), 2015.
- [15] Y. SHEN AND O. ZIKANOV. Thermal convection in a liquid metal battery. *Theoretical and Computational Fluid Dynamics*, vol. 30 (2016).
- [16] D. KEOGH, *et al.* Modelling the effects of areal capacity on mass transport in liquid metal batteries. *Journal of Power Sources*, vol. 573 (2023), p. 233142.

- [17] P. PERSONNETAZ, *et al.* Thermally driven convection in li—bi liquid metal batteries. *Journal of Power Sources*, vol. 401 (2018), pp. 362–374.
- [18] D.H. KELLEY AND D.R. SADOWAY. Mixing in a liquid metal electrode. *Physics of Fluids*, vol. 26 (2014), no. 5, p. 057102.
- [19] A. BELTRÁN. MHD natural convection flow in a liquid metal electrode. *Applied Thermal Engineering*, vol. 114 (2017), pp. 1203–1212.
- [20] A. BELTRÁN, J. NÚÑEZ, AND I. ALFONSO. Electromagnetically driven flow of weak electrolyte with liquid metal stratified in a cylindrical container: experimental study. *Magnetohydrodynamics*, vol. 56 (2020), pp. 113–120.
- [21] K. ACOSTA-ZAMORA AND A. BELTRÁN. Study of electromagnetically driven flows of electrolytes in a cylindrical vessel: Effect of electrical conductivity, magnetic field, and electric current. *International Journal of Heat and Mass Transfer*, vol. 191 (2022), p. 122854.
- [22] O. LAMINI, W. RUI, AND Z. CHANGYING. Experimental study on the effect of the liquid/surface thermal properties on droplet impact. *Thermal Science*, vol. 25 (2020), pp. 142–142.
- [23] Y. PLEVACHUK, *et al.* Thermophysical properties of the liquid gainsn eutectic alloy. *Journal of Chemical and Engineering Data*, vol. 59 (2014), p. 757763.
- [24] H. ROSSBY. A study of Bénard convection with and without rotation. *Journal of Fluid Mechanics*, vol. 36 (1969), pp. 309–335.
- [25] S. GLOBE AND D. DROPKIN. Natural-Convection Heat Transfer in Liquids Confined by Two Horizontal Plates and Heated From Below. *Journal of Heat Transfer*, vol. 81 (1959), no. 1, pp. 24–28.
- [26] T. AGUILAR-GARCÍA, *et al.* Effect of electromagnetically driven liquid metal flows on the electric potential difference in a cuboid vessel. *Journal of Power Sources*, vol. 483 (2021), p. 229162.

Received 24.11.2024